AFRL-RY-WP-TP-2010-1151

A NONLINEAR-PHASE, MODEL-BASED HUMAN DETECTOR FOR RADAR (PREPRINT)

S.Z. Gürbüz, W.L. Melvin, and D.B. Williams

Georgia Tech Research Institute

JUNE 2010

AIR FORCE RESEARCH LABORATORY
SENSORS DIRECTORATE
WRIGHT-PATTERSON AIR FORCE BASE, OH 45433-7320
AIR FORCE MATERIEL COMMAND
UNITED STATES AIR FORCE

REPORT DOCUMENTATION PAGE

Form Approved
OMB No. 0704-0188

1. REPORT DATE *(DD-MM-YY)*	2. REPORT TYPE	3. DATES COVERED *(From - To)*
June 2010	Technical Paper Preprint	08 September 2006 – 31 August 2009

4. TITLE AND SUBTITLE
A NONLINEAR-PHASE, MODEL-BASED HUMAN DETECTOR FOR RADAR (PREPRINT)

5a. CONTRACT NUMBER
FA8650-05-D-1912-0007

5b. GRANT NUMBER

5c. PROGRAM ELEMENT NUMBER
62204F

6. AUTHOR(S)
S.Z. Gürbüz, W.L. Melvin, and D.B. Williams

5d. PROJECT NUMBER
7622

5e. TASK NUMBER
11

5f. WORK UNIT NUMBER
7622110P

7. PERFORMING ORGANIZATION NAME(S) AND ADDRESS(ES)
Georgia Institute of Technology
School of Electrical and Computer Engineering
Georgia Tech Research Institute
Atlanta, GA

8. PERFORMING ORGANIZATION REPORT NUMBER

9. SPONSORING/MONITORING AGENCY NAME(S) AND ADDRESS(ES)
Air Force Research Laboratory
Sensors Directorate
Wright-Patterson Air Force Base, OH 45433-7320
Air Force Materiel Command
United States Air Force

10. SPONSORING/MONITORING AGENCY ACRONYM(S)
AFRL/RYRR

11. SPONSORING/MONITORING AGENCY REPORT NUMBER(S)
AFRL-RY-WP-TP-2010-1151

12. DISTRIBUTION/AVAILABILITY STATEMENT
Approved for public release; distribution unlimited.

13. SUPPLEMENTARY NOTES
Technical paper. PAO Case Number: 88ABW-08-0770; Clearance Date: 30 Oct 2008. Paper contains color.

14. ABSTRACT
Radar offers unique advantages over other sensors for the detection of humans, such as remote operation during virtually all weather and lighting conditions. Many current radar-based human detection systems employ some type of Fourier analysis, such as spectrograms. However, in many environments, the signal-to-noise ratio (SNR) for human targets is quite low and the spectrogram is almost completely masked by clutter. Furthermore, Fourier-based techniques assume a linear target phase, whereas human targets have a highly nonlinear phase history. The resulting phase mismatch causes significant SNR loss in the detector itself. In this paper, human modeling is used to derive a more accurate non-linear approximation to the true target phase history. The likelihood ratio is optimized over unknown model parameters to enhance detection performance. Cramer-Rao bounds (CRB) on parameter estimates and receiver operating characteristic (ROC) curves are used to validate analytically the performance of the proposed method and to evaluate simulation results.

15. SUBJECT TERMS
human detection, radar signal processing, synthetic aperture radar, detection and estimation

16. SECURITY CLASSIFICATION OF:			17. LIMITATION OF ABSTRACT:	18. NUMBER OF PAGES	19a. NAME OF RESPONSIBLE PERSON (Monitor)
a. REPORT	b. ABSTRACT	c. THIS PAGE			Nivia Colon-Diaz
Unclassified	Unclassified	Unclassified	SAR	18	19b. TELEPHONE NUMBER *(Include Area Code)* N/A

Standard Form 298 (Rev. 8-98)
Prescribed by ANSI Std. Z39-18

A Nonlinear-Phase, Model-Based Human Detector for Radar

Sevgi Z. Gürbüz, *Student Member, IEEE,* William L. Melvin, *Fellow, IEEE,* and Douglas B. Williams, *Senior Member, IEEE*

***Abstract*—Radar offers unique advantages over other sensors for the detection of humans, such as remote operation during virtually all weather and lighting conditions. Many current radar-based human detection systems employ some type of Fourier analysis, such as spectrograms. However, in many environments, the signal-to-noise ratio (SNR) for human targets is quite low and the spectrogram is almost completely masked by clutter. Furthermore, Fourier-based techniques assume a linear target phase, whereas human targets have a highly nonlinear phase history. The resulting phase mismatch causes significant SNR loss in the detector itself. In this paper, human modeling is used to derive a more accurate non-linear approximation to the true target phase history. The likelihood ratio is optimized over unknown model parameters to enhance detection performance. Cramer-Rao bounds (CRB) on parameter estimates and receiver operating characteristic (ROC) curves are used to validate analytically the performance of the proposed method and to evaluate simulation results.**

***Index Terms*—Human detection, radar signal processing, synthetic aperture radar, detection and estimation.**

I. Introduction

Over the last decade a variety of Fourier-based techniques have been applied to detect human targets in differing situations using radar. For example, Yarovoy [1] used ultra-wide band (UWB) radar to locate humans trapped in buildings by sensing respiratory motions. The radar returns from breathing and non-breathing targets were separated by analyzing the spectral variations of the radar return. Falconer [2] utilized differences in the shape of the power spectral density (PSD) of the return signal from a pulsed-Doppler microwave radar placed outside a building to differentiate between targets and infer the activity level of humans inside, discerning only large movements. Sabatini [3] applied wavelet analysis to the time varying-range profile measured with sonar to find human targets. All of these aforementioned techniques attempt to pick out probable human targets by identifying low-frequency periodic motion, which can be confused with the motion of other non-human targets, such as a slowly spinning ceiling fan.

The first attempts at developing detection algorithms that focused on features unique to human targets began with work by Weir [4] in 1997, where he developed the concept of a "gait velocitygram" – the velocity profile of a human target as seen by a sonar, or ultrasonic ranging device. The velocitygram contained distinct features that were used to calculate gait parameters, such as walking speed, cadence, step length, step time, and time to steady state walking. Indeed, work on gait analysis using visual and seismic sensors has led researchers to suggest that the human gait may become a biometric parameter that could be used for identification, just like fingerprints or hand geometry [5].

Frequency-based concepts were refined with the concept of the "radar gait signature" – a spectral analysis of the gait signature that has been shown to be characteristic of humans [5,6,7,8,10]. Although Geisheimer [6] initially used chirplet transforms to characterize the gait signature, spectrograms have been proposed as a simpler way of extracting biomechanical information from the radar return. In 2002, Geisheimer [7] experimentally verified that the overall spectrogram from a human target matched the sum of spectrograms constructed from the returns of individual body parts. The theoretical basis for this result was developed by Van Dorp [8], who divided the human body into 12 parts and computed the time-varying range for each part using a walking model developed by Thalmann [9]. Van Dorp showed that the human model-based simulated gait signatures matched the spectrograms derived from measured data – an important result that will serve as the basis for the human model utilized in this paper.

This foundation has led to much work that exploits the unique features of the human spectrogram. For example, Otero [10] used the spectrogram to compute features such as the stride and appendage/torso ratio. Plotting the velocity and appendage/torso ratio for pedestrians passing by, Otero observed that male and female targets were roughly grouped in different regions on the grid, suggesting that such features may be used for gender discrimination. As another example, Greneker [11] exploited the changes in stride and velocity caused by the weight of a load around the waist to propose a

Manuscript received October x, 2008. This work was supported in part by the U.S. Air Force Research Laboratory under prime contract FA8650-05-D-1912 and approved for Public Release as xxxx.

S. Z. Gürbüz is with the School of Electrical and Computer Engineering, Georgia Institute of Technology, Atlanta, GA 30332-0250 USA (email: sevgi@alum.mit.edu)

W. L. Melvin, is with the Georgia Tech Research Institute, Georgia Institute of Technology, Atlanta, GA 30301 USA (e-mail: bill.melvin@gtri.gatech.edu).

D. B. Williams is with the School of Electrical and Computer Engineering, Georgia Institute of Technology, Atlanta, GA 30332-0250 USA (e-mail: dbw@ece.gatech.edu).

spectrogram-based suicide bomber detection system.

These techniques aim at applying spectrograms to characterize targets already detected through Doppler or Fourier-based processing and were used in close proximity to the target or in situations where interference was minimal. In practice, spectrograms are often completely obscured in high clutter environments, rending impossible the accurate estimation of any feature or parameter that is to be used to discriminate humans from other targets [12]. Moreover, since human targets have relatively weak returns in comparison to vehicles or other objects, detecting even the existence of a human target is more difficult. In the event that a detector fails to detect a probable human target, any of the above characterization techniques cannot be applied.

Note that the Fourier transform implements a linear-phase filter yielding a peak response only when the target phase is also linear. In fact, the phase history for human targets is non-linear [13], so that the resulting phase mismatch causes a significant loss in output signal-to-noise ratio (SNR) inherent to the detector as the dwell increases, thereby degrading detection performance.

The goal of this paper is to derive a new, nonlinear-phase detector such that the phase mismatch between detector and target phase is minimized, and thus output SNR and probability of detection are maximized. In Section II, Thalmann's kinematic model for human walking is used as a basis for deriving an analytic expression of the true human target phase and for generating the synthetic human radar data used in our computer simulations. The deficiency of linear phase detectors is evaluated in Section III, which introduces spectrograms and analyzes the output signal-to-noise ratio (SNR) losses of Fourier-based methods. In Section IV, the proposed human model-based optimized nonlinear phase (ONLP) detector is derived. Maximum likelihood estimates (MLE) of unknown geometry and model parameters are obtained to maximize the likelihood ratio and resulting matched filter output. Cramer-Rao bounds of parameter estimates are used to illustrate the impact of modeling error on performance. Finally, in Section V, the detection performance of FFT-based matched filters is compared to that of the proposed ONLP detector, as well as to the ideal "clairvoyant" detector, representing the best performance attainable with complete knowledge of target parameters.

II. Signal Modeling

A. Received Signal

In general, the received radar signal is a time-delayed, frequency-shifted version of the transmitted chirp signal. Then the return for a point target may be expressed as

$$s_r(n,t) = a_t\, rect\left(\frac{\hat{t}-t_d}{\tau}\right) e^{j[-2\pi f_c t_d + \pi\gamma(\hat{t}-t_d)]}, \quad (1)$$

where the time t is defined as $t = T(n-1)+\hat{t}$ in terms of the pulse repetition interval (PRI), T, the pulse number, n, and the time relative to the start of each PRI, $\hat{t}$; a_t is the amplitude as given by the radar range equation; τ is the pulse width; c is the speed of light; γ is the chirp slope; f_c is the transmitted center frequency; and t_d is the round trip time delay between antenna and target, defined in terms of the target range, R, as $t_d = 2R/c$.

Exploiting the work of Geisheimer and Van Dorp, who showed that a human target could be divided into parts and the total response obtained by simply summing the responses of each part – i.e., that the principle of superposition could be applied to human modeling – the radar return from a human target may be mathematically expressed as

$$s_h(n,t) = \sum_{i=1}^{K} a_{t,i}\, rect\left(\frac{\hat{t}-t_{d,i}}{\tau}\right) e^{j[-2\pi f_c t_{d,i} + \pi\gamma(\hat{t}-t_{d,i})]}, \quad (2)$$

where K are the number of point targets comprising the overall human target.

The amplitude $a_{t,i}$, defined as

$$a_{t,i} = \frac{G\lambda\sqrt{P_t\sigma_i}\,\sigma_n}{(4\pi)^{1.5} R_i^2 \sqrt{L_s}\sqrt{L_a}\sqrt{T_{sys}}}, \quad (3)$$

includes several factors which vary with target range, R_i, and geometry. For instance, the antenna gain, G, varies according to angle of incidence, and the atmosphere losses, L_a, vary with range. For simplicity, we assume that these parameters are constant, along with the transmitted signal power, P_t, the wavelength, λ, the system loss, L_s, the system temperature, T_{sys}, and the noise standard deviation, σ_n. The radar cross section (RCS), σ_i, is modeled according to the shapes of the body parts. Thus, the head is modeled as a sphere and the other body parts as cylinders.

B. Human Model

A human is a complicated target because of the intricate motion of body parts moving along different trajectories at different speeds. In this work, the human body is divided into twelve basic body parts: the head, upper arms, lower arms, torso, thighs, lower legs and feet. As indicated in Fig. 1, each point target is taken to lie at the center of the corresponding body part.

The time-varying position of each point target may be computed using the kinematic model of a walking human developed by Thalmann [9]. In the Thalmann model, all positions are referenced to the base of the spine, denoted by

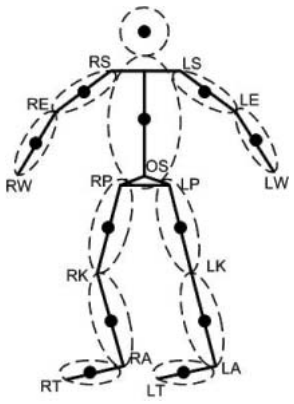

Figure 1. 12-point human model [12].

OS. Over the course of one cycle (two steps), the vertical, lateral, and translational position of OS varies sinusoidally. The time-varying angles of the joints are also provided by means of charts and equations in [9]. Together with the dimensions of the human body, these time-varying joint angles may be used to compute the time-varying positions of each point target relative to OS and each of the time delays ($t_{d,i}$) required in (2).

C. Data Generation

To test and evaluate the proposed algorithms, the radar signal and human model equations described above are used to generate simulated radar data in MATLAB. The slow-time, fast-time data matrix is pulse compressed so that the peak occurs at the range bin in which the target is present. Taking a slice across slow-time at the range bin of the peak output,

$$x_p[n] = \sum_{i=1}^{12} a_{t,i} e^{-j\frac{4\pi f_c}{c} R_{d,i}}, \qquad (4)$$

where $R_{d,i}$ is the range from the antenna to the center of each body part.

Spectrogram-based algorithms as well as the new method proposed in this paper use the slow-time slice in (4) as the starting point for data processing.

III. HUMAN SPECTROGRAMS

A. Computation

The spectrogram of a human target may be computed by stacking the fast Fourier transforms (FFT) of short, overlapping time segments taken from the slow-time slice in (4). An example of the simulated spectrogram for a human target is shown in Fig. 2.

The strongest return is received from the torso, with its low-frequency, small-amplitude sinusoidal oscillatory motion. The appendages that travel the farthest during the walking cycle – the feet – appear in the spectrogram with the largest amplitude oscillation. Note that the special nature of the periodicities within the human spectrogram are what makes this response unique and differentiable from the spectrograms of even other animals, as can be seen from the measured spectrograms of a human and dog given by Otero in [10]. The human spectrogram measured by Otero also compares well with the spectrograms generated based on our human model.

In many practical environments, however, the impact of clutter and noise is significant in masking human targets, which are weak in comparison to other objects with higher RCS, such as automobiles. When the pulse-wise SNR drops to -15dB, even the torso return is difficult to discern (Fig. 3). Thus, for many practical radar problems, the spectrogram is of little help in discriminating human targets from other objects.

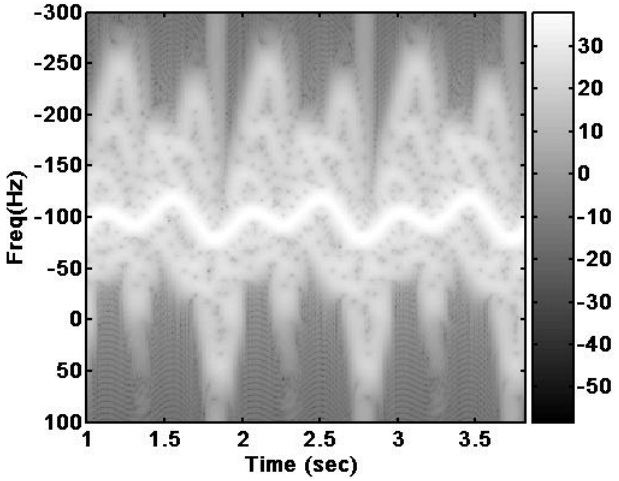

Figure 2. Simulated human spectrogram.

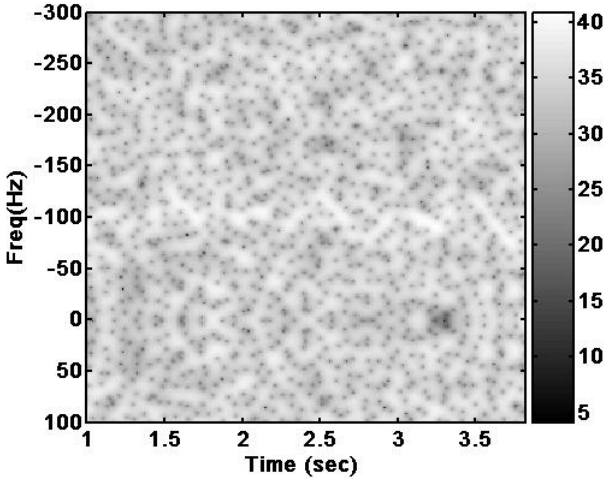

Figure 3. Human spectrogram in noise with SNR = -15dB.

B. Inherent SNR loss in Fourier-based detectors

More importantly, the Fourier transforms used in calculating the spectrogram or in Doppler processing are inherently linear phase matched filters. However, the phase history of a human target can be highly nonlinear, resulting in an inherent SNR loss when matched filtered with a linear-phase filter, such as the FFT. Consider the phase history of a typical human target

walking at a 45° incidence angle relative to the initial antenna-target vector, as shown in Fig. 4. At first glance, the phase does not appear to be highly non-linear and it would seem that the FFT should be a good match. In fact, as is shown in Section IV, for human targets the phase history is comprised of a linear as well as oscillatory component. Subtracting out the linear component of the phase in Fig. 4, the oscillatory components are revealed (Fig. 5).

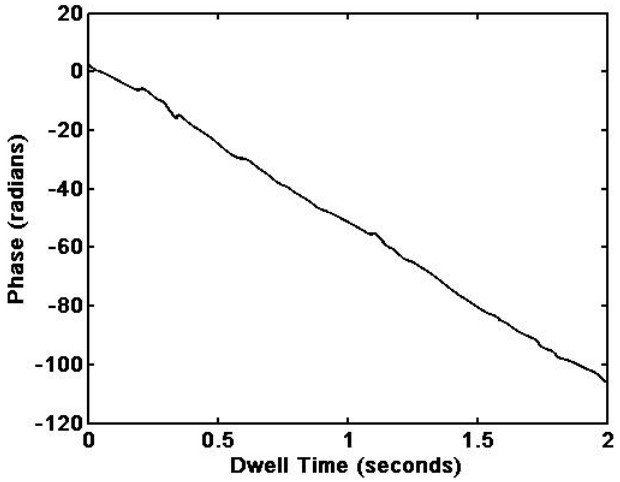

Figure 4. Phase history of a typical human target walking along a vector maximally aligned with the initial antenna-target vector.

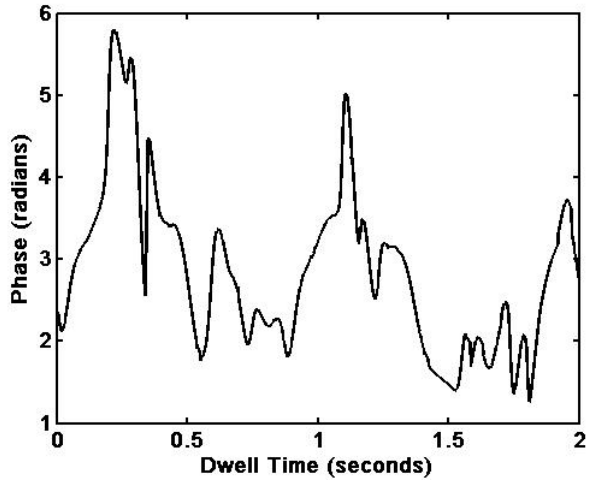

Figure 5. Phase history of Fig. 4 after linear component is removed.

The SNR loss incurred may be quantitatively analyzed as follows. Define the true target data as

$$\mathbf{s} = \begin{bmatrix} \alpha_0 & \alpha_1 e^{j\theta_1} & \cdots & \alpha_{N-1} e^{j(N-1)\theta_{N-1}} \end{bmatrix}^T \qquad (5)$$

where N is the total number of pulses transmitted, and α_i and θ_i are generalized amplitude and phase factors, respectively. Note that in general both the amplitude and phase factors vary with slow-time (*n*).

When filtered with the weight vector, *w[n]*, the output SNR is

$$SNR = \frac{E[\mathbf{w^H s s^H w}]}{E[\mathbf{w^H x_n x_n^H w}]} \qquad (6)$$

where $\boldsymbol{x_n}$ is the noise signal. If we assume that the noise has a covariance matrix of $\sigma_n^2\mathbf{I}$, then (6) may be simplified to

$$SNR = \frac{\left|\mathbf{w^H s}\right|^2}{\sigma_n^2 \left|\mathbf{w^H w}\right|} \qquad (7)$$

The maximum output SNR is attained when the received signal $\boldsymbol{s}$ is matched filtered against itself:

$$SNR_0\big|_{\mathbf{w}=\mathbf{s}} = \frac{1}{\sigma_N^2}\mathbf{s^H s} \qquad (8)$$

However, since knowing the target return exactly in advance is impossible, current systems typically matched filter with a linear phase filter, which may be expressed as

$$\mathbf{w_{LIN}} = \begin{bmatrix} \beta_1 & \beta_2 e^{j\phi} & \cdots & \beta_{N-1} e^{j(N-1)\phi} \end{bmatrix}^T, \qquad (9)$$

where β_i and ϕ are generalized amplitude and phase parameters, respectively. Here, the amplitude factor is left in a general form that varies with slow-time, while only the phase has been restricted as linear. The output SNR for such a linear phase filter is

$$SNR_{LIN}\big|_{\mathbf{w}=\mathbf{w}_{\mathbf{LIN}}} = \frac{\left|\mathbf{w_{LIN}^H s}\right|^2}{\sigma_N^2 \left|\sum_{n=0}^{N-1} \beta_n^2\right|} \qquad (10)$$

Thus, the SNR loss incurred from signal mismatch is

$$SNR\ Loss = \frac{SNR_{LIN}}{SNR_0} = \frac{\left|\mathbf{w_{LIN}^H s}\right|^2}{\left|\sum_{n=0}^{N-1} |\beta_n|^2\right| \mathbf{s^H s}} \le 1 \qquad (11)$$

There are three main factors which impact SNR loss: phase mismatch, amplitude mismatch, and dwell time. Fig. 6 illustrates the affect of these factors by applying Fourier processing on the example phase history of Fig. 4, which has an amplitude variation of $2.64\text{x}10^{-7} \pm 2.5\text{x}10^{-7}$ over a 2 second dwell. The FFT computes a constant, flat-line approximation

to the true amplitude, i.e. $\beta_n=\beta$ for all n. But the amplitude mismatch – defined as the SNR loss incurred due to amplitude differences, assuming identical phase – is not nearly as significant as the phase mismatch. Over a 2 second dwell, the phase moves through 100 radians, or 5732 degrees, of phase. However, just a 1% error in the slope causes the phase to shift by 2π, an entire cycle. Thus, unlike the amplitude, phase is extremely sensitive to mismatch; despite the gross linear appearance of the phase history, the underlying nonlinearities that are invisible to the naked eye in fact result in SNR losses of up to 30 dB for a 2 second dwell time.

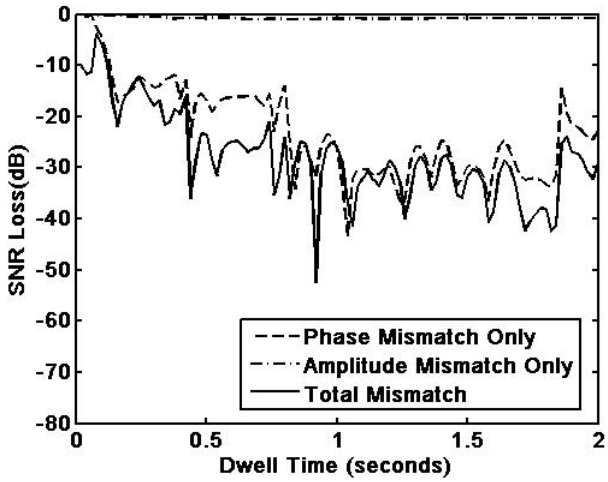

Figure 6. SNR Loss variation over dwell time for the target phase history shown in Fig. 4.

Collecting data over a longer dwell, so that the integration gain increases, also does not help alleviate the inherent SNR loss in Fourier-based, linear phase detectors. Consider the plot in Fig. 7, which shows the trend of the output SNR normalized by input SNR as dwell time is increased for both the ideal, clairvoyant detector and the FFT. While the output SNR continually increases with dwell for the clairvoyant detector, the FFT exhibits on average a flat trend, so that the output SNR does not significantly increase with dwell time. Indeed, the SNR loss, as shown by the difference between the two curves in Fig. 7, simply increases with dwell.

Thus, matched filtering with a more accurate model of the signal phase history has the potential to yield a significant reduction in output SNR losses and, thereby, substantially improve detection performance. For this same example, the model-based optimized nonlinear phase (ONLP) detector proposed in this paper exhibits an SNR loss of only 7 dB for a 2 second dwell time.

The remaining sections of this paper focus on the design and performance of the ONLP detector.

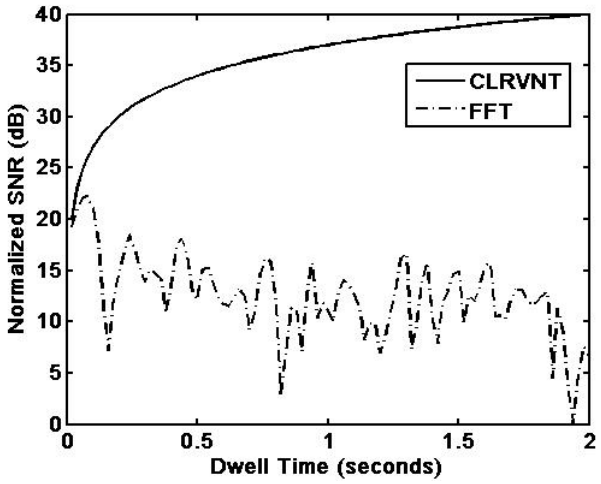

Figure 7. Output SNR variation over dwell time normalized by input SNR for the target phase history shown in Fig. 4 comparing clairvoyant and FFT-based detectors.

IV. DETECTOR DESIGN

A. Detector Formulation

For each range bin centered at r_b, the detector must make a decision between two hypotheses:

$$\begin{aligned} H_0 &: \quad \mathbf{x} = \mathbf{x_n} \\ H_1 &: \quad \mathbf{x} = \mathbf{s} + \mathbf{x_n} \end{aligned} \tag{12}$$

where $\mathbf{x_n}$ is complex Gaussian noise with covariance matrix $\mathbf{R_I}$, $\mathbf{s}$ is the true target signal, and we've assumed that there is no range migration, i.e., the entire target return is contained within one range bin. Since the noise covariance matrix cannot be known apriori, an estimate must be used instead. In this paper, we assume clairvoyance:

$$\hat{\mathbf{R}}_\mathbf{I} = \mathbf{R}_\mathbf{I} = \sigma_n^2 \mathbf{I}, \tag{13}$$

where σ_n^2 is the noise power.

A likelihood ratio test [14, 15] is used to determine the detector decision rule. Under H_0, the noise is distributed as CN($\mathbf{0}, \hat{\mathbf{R}}_\mathbf{I}$) while under H_1 the noise distribution is CN($\mathbf{s}, \hat{\mathbf{R}}_\mathbf{I}$), where $\mathbf{s}=\mathbf{x_p}$ is the target signal vector. Thus the decision rule may be expressed as

$$\text{Decide } H_1 \text{ if } \frac{p(\mathbf{x};H_1)}{p(\mathbf{x};H_0)} > \gamma \rightarrow \text{Re}\left\{\mathbf{s}^\mathbf{H}\hat{\mathbf{R}}_\mathbf{I}^{-1}\mathbf{x}\right\} > \gamma' \tag{14}$$

where $\gamma' = \sqrt{\text{Re}\{\mathbf{s}^\mathbf{H}\hat{\mathbf{R}}_\mathbf{I}^{-1}\mathbf{s}\}} \cdot Q^{-1}(P_{FA})$ and P_{FA} is the desired probability of false alarm.

Since the target return, **s**, is not known apriori, a realizable detector must use an approximation. Our goal in this paper is to develop a better approximation to the target return than that of the linear-phase FFT so as to minimize SNR loss and achieve better detection performance.

The human-model based expression for the target return in (4) is a very good approximation to the true target signal, **s**; however, this model is much too complicated for use as an effective matched filter. The model contains over 24 unknown parameters and most of the kinematic expressions used to compute the time-varying range of each body part are not presented in closed form, but rather as graphs, which must be combined with other charts or equations to derive the time-varying position [9]. Thus, we next derive a simpler, non-linear approximation to (4) that will serve as the basis for our proposed optimized non-linear phase (ONLP) detector.

B. Approximating Expected Target Return

As shown in Fig. 2, the torso response is significantly stronger than the response from the remaining eleven body parts comprising the model, so we will simplify first by neglecting the motion of all body parts except the torso, i.e. we will design the detector to match as best as possible the response from the torso only.

Furthermore, since the overall SNR loss is caused primarily by phase mismatch, we will approximate the received signal amplitude, a_t, as a being constant, A, even though there is some variation across slow-time due to slight variations in gain, RCS, and other loss factors. We also approximate the range term in the amplitude factor (3) with r_b, the center of the range bin at which the peak pulse compression output occurred.

For the range term in the phase, however, we cannot make as crude an approximation, because the phase is much more sensitive to errors than the amplitude. A more accurate approximation to range is obtained as follows.

Define $\boldsymbol{r_1}$ as the vector from the antenna to the target's initial position and $\boldsymbol{r_N}$ as the vector from the antenna to the target's final position. For simplicity, assume that the human motion is linear along a constant angle, θ, relative to $\boldsymbol{r_1}$. Then the vector $\boldsymbol{h}$ between the initial and final target locations represents the human motion (Fig. 8).

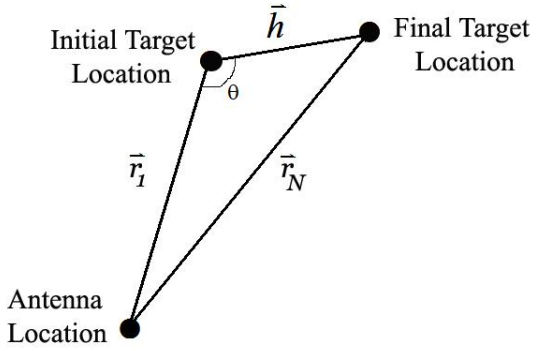

Figure 8. Antenna-target geometry.

Using the law of cosines, we may write

$$|\mathbf{r_n}|^2 = |\mathbf{r}_1|^2 + |\mathbf{h}|^2 - 2|\mathbf{r_1}||\mathbf{h}|\cos\theta\,. \tag{15}$$

Since $|\mathbf{h}| << |\mathbf{r_1}|$ and $\sqrt{1+x} \approx 1 + x/2$ for small x,

$$|\mathbf{r_n}| \approx |\mathbf{r_1}| - |\mathbf{h}|\cos\theta\,. \tag{16}$$

Then, (4) may be written as

$$x_p[n] \approx \frac{A}{r_b^2} e^{-j\frac{4\pi f_c}{c}(r - h\cos\theta)}, \tag{17}$$

where r = $|\mathbf{r_1}|$ and h = $|\mathbf{h}|$.

The human motion vector $\boldsymbol{h}$ may be more explicitly expressed using the Thalmann kinematic equations as

$$h^2 = OS_V^2 + OS_L^2 + \left(vTn + OS_{FB}\right)^2, \tag{18}$$

where

$$OS_V = 0.015RV\left[-1 + \sin\left(4\pi t\% - 0.7\pi\right)\right]$$

$$OS_L = A_L \sin\left(2\pi t\% - 0.2\pi\right)$$

$$A_L = \begin{cases} -0.032 & \text{for } 0.5 < RV < 2.3 \\ -0.128RV^2 + 0.128 & \text{for } RV < 0.5 \end{cases}$$

$$OS_{FB} = A_a \sin\left(4\pi t\% + 2\phi_a\right)$$

$$A_a = \begin{cases} -0.021 & \text{for } 0.5 < RV < 2.3 \\ -0.084RV^2 + 0.084RV & \text{for } RV < 0.5 \end{cases}$$

$$\phi_a = -0.127 + 0.731\sqrt{RV}$$

Here, OS_L, OS_V, and OS_{FB} represent the lateral, vertical and forward/backward motion of the center of the torso relative to coordinate origin of OS (see Fig. 1) located at the base of the spine. The Thalmann equations depend on only two variables: 1) RV, the ratio of velocity (v) to thigh height (HT); and, 2) t%, a time index taken relative to the beginning of a step. Mathematically, these variables may be expressed as

$$RV = \frac{v}{HT} \tag{19}$$

and

$$t\% = \frac{nT}{1.346}\sqrt{RV} + t_0\,, \tag{20}$$

where t_0 is a constant indicating the point within the stepping cycle that the first transmitted pulse reflects from the target.

The expression for h may be simplified by throwing out second order terms and approximating the square root as

$$\begin{aligned} h &\approx \sqrt{(vTn)^2 + 2vTnOS_{FB}} \\ &= vTn\sqrt{1+\frac{2OS_{FB}}{vTn}} \approx vTn + OS_{FB}. \end{aligned} \quad (21)$$

This equation is consistent with the phase histories plotted previously in Fig. 4 and Fig. 5. For small radial velocities, v, the oscillatory term dominates, whereas for large v, the linear term dominates, masking the underlying nonlinearity.

Although generally speaking the phase will contain multiple sinusoids as a result of the quadratic components we previously neglected in (18), too detailed a model will render the detector fragile under noise, so just one sinusoid is used as a nonlinear approximation to the true target phase.

Mathematically, then, the ONLP approximation to the true target phase is

$$x_{onlp}[n] = \frac{A}{r_b^2} e^{j\left(Mn + C_1 + C_2\cos(C_3 n + C_4)\right)}, \quad (22)$$

with M, the slope proportional to Doppler frequency; C_1, a factor dependent upon range; C_2, the amplitude of torso motion; C_3, torso frequency; C_4, torso phase; and A, the amplitude as defined in the range equation. These variables are unknown model parameters over which the matched filter response will be optimized.

C. Estimating Model Parameters

The maximum likelihood estimate (MLE) for the any parameter ξ_i in a signal $\boldsymbol{x}$ with mean μ in complex Gaussian noise may be expressed as [16]

$$\frac{\partial \ln\left(p(\mathbf{x};\boldsymbol{\xi})\right)}{\partial \xi_i} = 2\,\mathrm{Re}\left\{\left(\mathbf{x}-\mu(\boldsymbol{\xi})\right)^H \mathbf{C}_\mathbf{x}^{-1}\frac{\partial \mu(\boldsymbol{\xi})}{\partial \xi_i}\right\}. \quad (23)$$

For ξ_i = A,

$$\frac{\partial \mu}{\partial A} = \frac{\partial x_{onlp}}{\partial A} = \frac{1}{r_b^2} e^{j\angle x_{onlp}}. \quad (24)$$

Thus, we set

$$\frac{\partial \ln\left(p(\mathbf{x};A)\right)}{\partial A} = \frac{2\,\mathrm{Re}\left\{\mathbf{x}^H e^{-j\angle \mathbf{x}_{\mathbf{onlp}}} - \frac{AN}{r_b^2}\right\}}{\sigma^2 r_b^2} = 0, \quad (25)$$

which in turn can be solved to find the MLE:

$$\begin{aligned} \hat{A} &= \frac{r_b^2}{N}\mathrm{Re}\left\{\mathbf{x}^H e^{-j\angle \mathbf{x}_{\mathbf{onlp}}}\right\} \\ &= \frac{r_b^2}{N}\mathrm{Re}\left\{\sum_{m=1}^{N} x_m e^{-jx_{onlp,m}}\right\} \end{aligned} \quad (26)$$

Although (23) may also be used to estimate the phase parameters, the resulting estimate is not numerically robust. Thus, the MLE for the phase parameters are instead found by first explicitly extracting the phase data. The phase of a complex signal may be found by taking the ratio of the imaginary and real parts. However, this operation also transforms the noise distribution from complex Gaussian to Cauchy, so that the problem may be restated as follows:

$$\begin{aligned} \tilde{H}_0 &: \quad \tilde{\mathbf{x}} = \tilde{\mathbf{x}}_\mathbf{n} \\ \tilde{H}_1 &: \quad \tilde{\mathbf{x}} = \tan\left(\angle \mathbf{x}_{\mathbf{onlp}}\right) + \tilde{\mathbf{x}}_\mathbf{n} \end{aligned} \quad (27)$$

where $\tilde{\mathbf{x}}_\mathbf{n}$ is Cauchy distributed noise. Thus, the distribution of $\tilde{\mathbf{x}}$ under H_1 may be computed to be

$$p\left(\tilde{\mathbf{x}};\tan(\angle \mathbf{x}_{\mathbf{onlp}})\right) = \frac{1/\pi^N}{\prod_{m=0}^{N-1}\left[1+\left(\tilde{x}_m - \tan(\angle x_{onlp,m})\right)^2\right]}, \quad (28)$$

where $\tilde{x}_m \equiv [\tilde{\mathbf{x}}]_m$, the m[th] element of $\tilde{\mathbf{x}}$.

The MLE for an unknown parameter ξ_i is given by solving the following equation for each ξ_i:

$$\frac{\partial}{\partial \xi_i}\ln p\left(\tilde{\mathbf{x}};\tan(\angle \mathbf{x}_{\mathbf{onlp}}),\gamma\right) = 0, \quad (29)$$

which can be reduced to

$$\sum_{m=0}^{N-1}\frac{\tilde{x}_m - \tan(\angle x_{onlp,m})}{1+\left(\tilde{x}_m - \tan(\angle x_{onlp,m})\right)^2}\frac{\partial}{\partial \xi_i}\tan(\angle x_{onlp,m}) = 0 \quad (30)$$

Computing of the MLE estimates for all 5 phase parameters thus requires solving a system of 5 nonlinear equations, which is impossible to do in closed form, and very computationally and memory intensive even when solved numerically.

Therefore, we break the problem into two stages by first estimating the linear component, and then estimating the non-linear term.

If in (17) we model the human motion as being simply that of a constant-velocity point target, then $h = nvT$ and

$$x_p[n] \approx \frac{A}{r_b^2} e^{-j\frac{4\pi f_c}{c}(r - nTv_r)}, \quad (31)$$

where $v_r = v\cos\theta$. The two unknown linear phase parameters r and v_r may then be found by solving the least squares problem $\mathbf{A\xi}=\mathbf{b}$ as

$$\hat{\boldsymbol{\xi}} = \left(\mathbf{A}^T\mathbf{A}\right)^{-1}\mathbf{A}^T\mathbf{b}, \quad (32)$$

where

$$\mathbf{A} = \frac{4\pi f_c}{c}\begin{bmatrix} T & 2T & \cdots & NT \\ -1 & -1 & \cdots & -1 \end{bmatrix}^T$$

$$\hat{\boldsymbol{\xi}} = \begin{bmatrix} r & v_r \end{bmatrix}^T$$

$$\mathbf{b} = \begin{bmatrix} \tan^{-1}(\tilde{x}_1) & \tan^{-1}(\tilde{x}_2) & \cdots & \tan^{-1}(\tilde{x}_N) \end{bmatrix}^T$$

An initial estimate of the slope M may then be found as

$$M_i = \frac{4\pi f_c}{c} T v_r = \frac{4\pi f_c}{c} T\hat{\xi}(2) \quad (33)$$

This initial estimate is then numerically refined so as to ensure no residual linear component remains.

Having computed an estimate for the slope M, the remaining parameters in the nonlinear component of the phase are estimated from (30), which is now reduced to a system of four nonlinear equations and four unknowns, solved using numerical iteration. Note that of these four parameters, the frequency and phase shift coefficients C_3 and C_4 are the most crucial for ensuring the best match between model and data. Thus, to save computation time, larger step sizes are used for C_1 and C_2, while finer step sizes are utilized for C_3 and C_4.

The final form of our proposed ONLP detector is

$$\mathrm{Re}\left\{\hat{\mathbf{x}}_{\mathbf{onlp}}^{\mathbf{H}}\hat{\mathbf{R}}_{\mathbf{I}}^{-\mathbf{1}}\mathbf{x}\right\} > \gamma' \quad (34)$$

where $\gamma' = \sqrt{\mathrm{Re}\{\hat{\mathbf{x}}_{\mathbf{onlp}}^{\mathbf{H}}\hat{\mathbf{R}}_{\mathbf{I}}^{-\mathbf{1}}\hat{\mathbf{x}}_{\mathbf{onlp}}\}}\cdot Q^{-1}(P_{FA})$, which is still a linear detector as the elements of $\boldsymbol{x}_{onlp}$ merely form the weights with which we filter our signal.

D. Quality of Parameter Estimates

Obtaining adequate estimates of the unknown model parameters is critical to the performance of the matched filter detector. The estimation problem, however, is affected by several factors, including the direction of motion (i.e. target geometry), dwell time, and SNR.

As indicated by (21), the phase history of a human target may be represented as the sum of linear and oscillatory components. Depending on the target geometry and walking speed, the shape of the phase history may vary. When the target moves roughly perpendicular to the antenna-target vector, the radial velocity will be nearly zero and the oscillatory component is clearly apparent. As the target moves along the antenna-target vector, the radial velocity is almost identical to the true target velocity, so the linear component has more of an affect.

The dwell time is also an important factor, as the amount of data collected limits the number of cycles we can observe. For example, at extremely short dwells, the phase history may only have a mild nonlinearity, similar to a bowed curve or a quarter-cycle of a sinusoid. Finally, SNR is also a critical factor, since as the noise level increases the true signal curvature is obscured, leading to degradation in our parameter estimates. For low SNRs, longer dwell times will be required for good parameter estimates.

The quality of the parameter estimates may be assessed using the Cramer-Rao Bound (CRB). It can be shown that for a general signal $x[n,\boldsymbol{\theta}]$ in complex Gaussian noise with variance σ^2, the CRB is given by [16]

$$\mathrm{var}\left(\hat{\theta}\right) \geq \frac{1}{I(\theta)\big|_{ij}} = \left[\frac{2}{\sigma^2}\mathrm{Re}\left\{\sum_{n=0}^{N-1}\frac{\partial x^H}{\partial\theta_i}\frac{\partial x}{\partial\theta_j}\right\}\right]^{-1}, \quad (35)$$

where $I(\boldsymbol{\theta})$ is the Fisher information matrix. Evaluating (34) for the expression of $\boldsymbol{x}_{onlp}$ given in (22), the desired CRB may be analytically expressed as

$$\mathrm{var}\left(\hat{\boldsymbol{\theta}}\right) \geq diag\left\{\frac{1}{4\cdot SNR}\mathbf{B}^{-1}\left(\hat{\boldsymbol{\theta}}\right)\right\} \quad (36)$$

where the pulse-wise SNR is defined as $A^2/2r_b^2\sigma^2$ and

$$B(\theta) = \begin{bmatrix} N & S_1 & C_2S_2 & C_2S_3 & 0 \\ S_1 & S_4 & C_2S_5 & C_2S_6 & 0 \\ C_2S_2 & C_2S_5 & C_2^2S_7 & C_2^2S_8 & 0 \\ C_2S_3 & C_2S_6 & C_2^2S_8 & C_2^2S_9 & 0 \\ 0 & 0 & 0 & 0 & \frac{N}{A^2} \end{bmatrix}$$

$$S_1 \equiv \sum_{n=0}^{N-1}\cos(C_3n + C_4); \quad S_2 \equiv \sum_{n=0}^{N-1} n\sin(C_3n + C_4)$$

$$S_3 \equiv \sum_{n=0}^{N-1}\sin(C_3n + C_4); \quad S_4 \equiv \sum_{n=0}^{N-1}\cos^2(C_3n + C_4);$$

$$S_5 \equiv \sum_{n=0}^{N-1} n\sin(C_3n + C_4)\cos(C_3n + C_4);$$

$$S_6 \equiv \sum_{n=0}^{N-1}\sin(C_3n + C_4)\cos(C_3n + C_4);$$

$$S_7 \equiv \sum_{n=0}^{N-1} n^2 \sin^2(C_3 n + C_4); \quad S_8 \equiv \sum_{n=0}^{N-1} n \sin^2(C_3 n + C_4);$$

$$S_9 \equiv \sum_{n=0}^{N-1} \sin^2(C_3 n + C_4).$$

In Fig. 9, the CRB on $\hat{C}_1$ is plotted together with the simulated variance of $\hat{C}_1$ under two cases: 1) The underlying data is exactly the same as the model $\mathbf{x}_{\mathbf{ONLP}}$ in (22) used to compute the CRB; and, 2) the underlying data is the synthetic human data representative of true human motion as given in (4). The MLE estimator achieves the performance of the

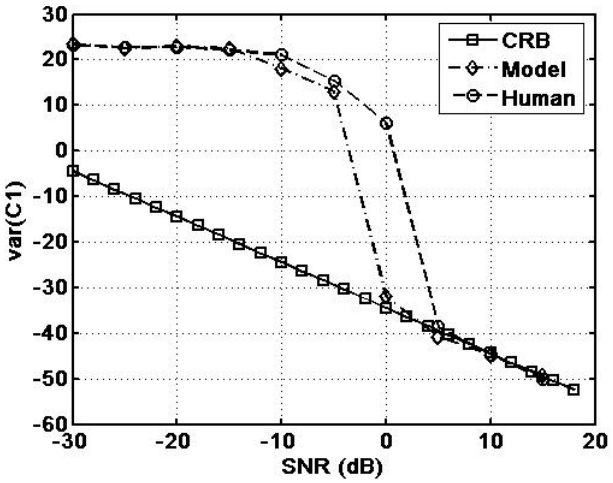

Figure 9. CRB and variance of parameter (C_1) MLE with ONLP approximation over 500 Monte Carlo trials.

CRB for single-pulse SNRs above 5 dB. Notice that for intermediate SNR values, there is a slight difference between the simulated variances when the model data and synthetic human data are used. For example, when the underlying data exactly matches the model, the estimates follow the CRB for SNRs above 0 dB. This 5 dB difference illustrates the impact of modeling error on the estimates. However, the fact that the variances match for most SNRs also validates the quality of the ONLP model in terms of approximating the true data.

The dwell time – i.e., the number of pulses transmitted during the entire data collect times the PRI – also has a significant impact on the quality of the parameter estimates. As illustrated in Fig. 10, the longer the dwell time, the better the estimate. Thus, when the SNR is very low, as is typical of human targets, data must be collected for a much longer time to achieve comparable performance to targets with a higher SNR (or RCS).

In this case, the estimate for the linear phase parameter, M, stabilizes after a 1.5 second dwell time when the SNR is 20 dB; but when the SNR is -20 dB, the estimate stabilizes after 2.4 seconds. In other words, for this particular example, to achieve the same quality of estimate, an additional 0.9 seconds of data must be collected.

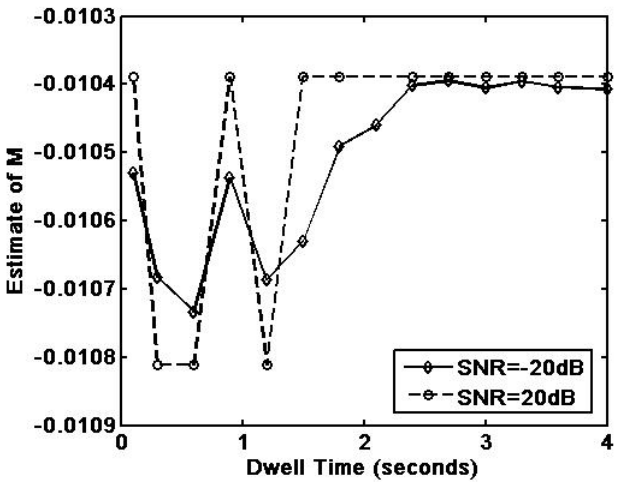

Figure 10. Variation of linear phase parameter, M, MLE versus number of pulses transmitted over 100 Monte Carlo trials.

V. PERFORMANCE

Detector performance is evaluated by applying the proposed ONLP detector to simulated radar data as generated in (4). The receiver operating characteristic (ROC) curves as well as the impact of SNR, incidence angle, and dwell time on the probability of detection (P_D) is assessed. By incidence angle, we mean the angle between the initial antenna-target vector and the target motion vector. Additionally, the effect on detection performance of multiple human targets within a single range bin is analyzed. The results presented in Fig. 11 – Fig. 15 are generated for a radar with the characteristics shown in Table 1.

TABLE 1

Center Frequency	1 GHz
Sampling Frequency	20 MHz
Bandwidth	10 MHz
Pulse Repetition Interval	0.2 ms
Pulse Width	40 μs
Transmit Power	1.8 kW
Nominal Range	8,760 m

A. Receiver Operating Characteristics

ROC curves for the clairvoyant, FFT, and ONLP detectors are shown for a human target walking parallel to the x-axis and with an incidence angle of 135° in Fig. 11. The proposed ONLP detector exhibits similar performance to the ideal clairvoyant detector at a PFA of 0.5, whereas the FFT never approaches ideal performance until the PFA is about 1. The ONLP performance exceeds that of the FFT for all PFAs.

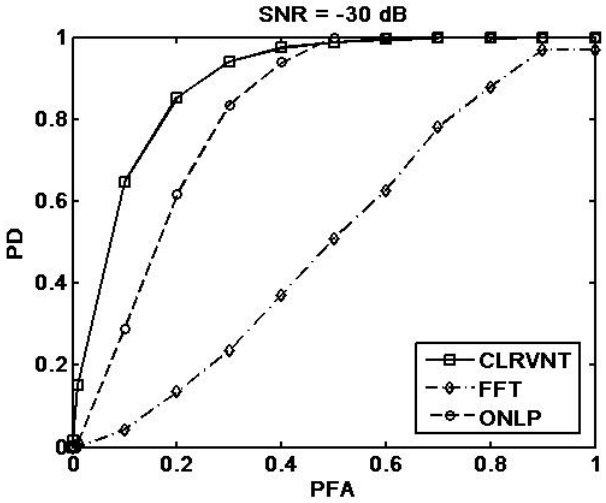

Figure 11. P_D vs. P_{FA} for a human target with an incidence angle of 135°, a dwell time of 0.5 s. and single-pulse SNR = -30dB.

B. Probability of Detection Versus SNR

The performance improvement of the proposed technique may also be seen in Fig. 12, which shows the affect of SNR on the probability of detection. The ONLP detector yields about an 11dB improvement in output SNR relative to the FFT.

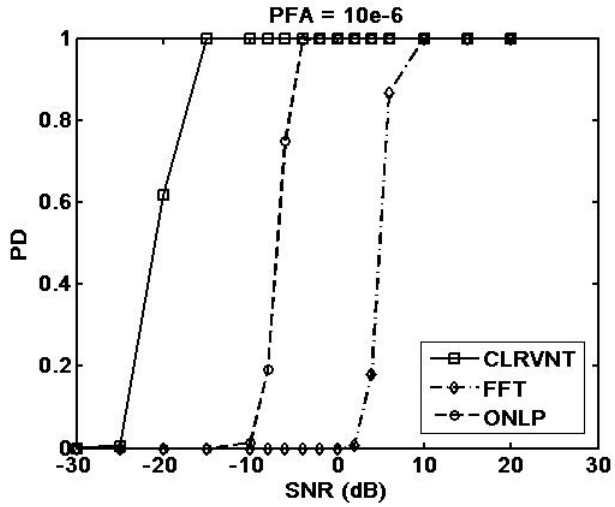

Figure 12. P_D vs. SNR for a human target with an incidence angle of 135°, a dwell time of 0.5 s. and $P_{FA}=10^{-6}$.

C. Impact of Target Motion on Detection

The ONLP method maintains this performance gain regardless of the target direction of motion. Fig. 13 shows the probability of detection variation over incidence angle for both the FFT and ONLP methods. Note that performance of the FFT plummets as that target's motion increasingly aligns with the radar-target vector. This is because as the radial velocity observed by the radar increases, the overall phase history becomes increasingly linear. Even a small error in estimating the phase history slope results in errors that accrue with dwell time and severely degrade performance. When the radial velocity is small, the phase history is predominantly sinusoidal and the phase mismatch errors are limited by the oscillation amplitude. Because the ONLP method optimizes the matched filter parameters, it maintains superior performance over all incidence angles.

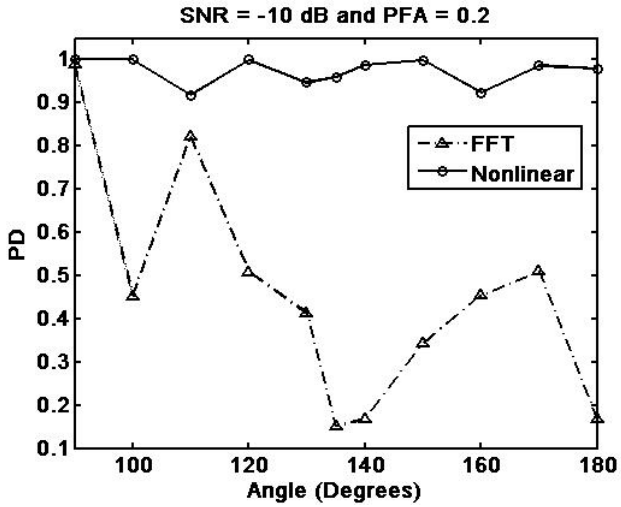

Figure 13. P_D vs. incidence angle for a human target with a dwell time of 0.5 s., SNR of -10dB and P_{FA}=0.2.

D. Probability of Detection Versus Dwell Time

The impact of dwell time on detection performance is shown in Fig. 14. After a dwell of about 1.2 seconds, the proposed ONLP detector achieves the same performance as the ideal, clairvoyant detector. However, the FFT-based detector is unable to detect any targets even after twice the dwell time. This result is consistent with expectations, as the output SNR versus dwell time plot of Fig. 7 also showed that for human detection FFT-based detectors do not exhibit improved performance with dwell time. By making a significantly better matched filter, however, not only are we able to achieve better detection performance at a given dwell time, but we are now able to eventually achieve ideal performance given a sufficiently long dwell.

E. Multi-Target Situation

Up until now, results have been provided for the case when a single target resides in a single range bin. However, considering human social patterns, more than one human target occupying the same range-bin is very likely, causing the phase history to, in fact, contain the sum of the phase information of multiple human targets. In this situation, we define a detection as the simple indication of a target present, not the determination of the number of targets present, a topic of future work.

Consider the case of three people starting at the same point, but walking in different directions: 45°, 0°, and -45° relative to x-axis. Then, the phase history obtained for a total number of 2,500 transmitted pulses consists of irregularly shaped oscillations, as shown in Fig. 15.

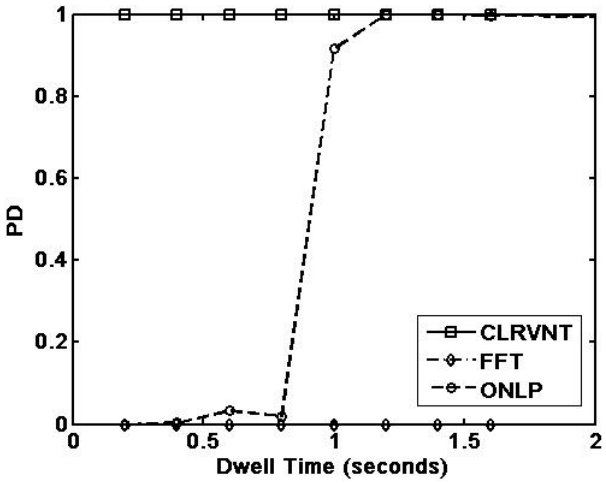

Figure 14. P_D v dwell time for a human target with an SNR of -10dB and $P_{FA}=10^{-6}$.

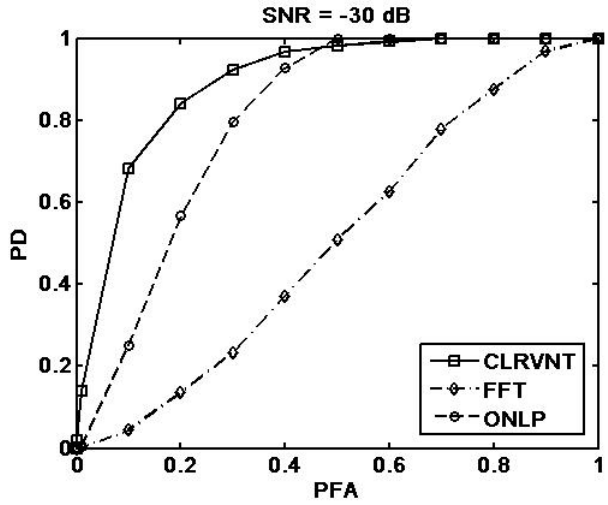

Figure 16. ROC curve comparing detector performance for the multi-target phase history of Fig. 15.

These irregularities do not significantly affect the detector design, as any nonlinearity is matched filtered with the best-fitting sinusoid, and thereby achieves improved detection performance, as shown in Fig. 16. Generally, the higher the number of targets in a range bin, the more complex and nonlinear the phase function. Although in an absolute sense, the degree to which the model matches the phase in the multi-target case may vary, the ONLP model will almost always better match the phase of – and thus outperform – the linear phase FFT.

VI. Conclusion

A novel method for improving the performance of matched-filters in detecting human targets has been presented. A sinusoidal (ONLP) approximation to the true target phase was derived based on the Thalmann human walking model, thereby capturing the characteristic nature of human motion. Results show a drastic improvement in output SNR and detection performance for the proposed method relative to existing FFT-based techniques.

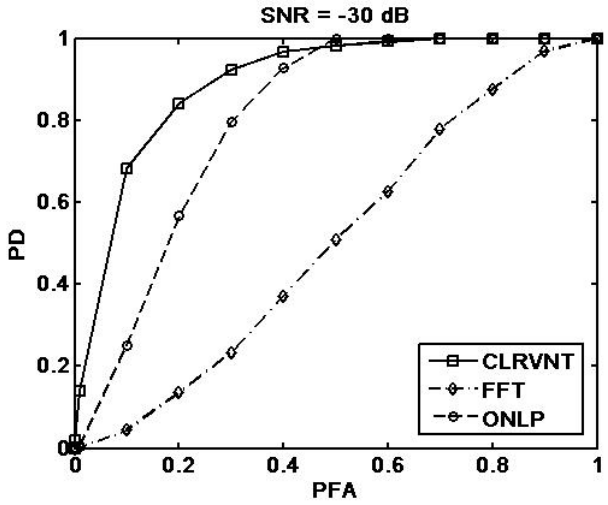

Figure 16. ROC curve comparing detector performance for the multi-target phase history of Fig. 15.

Possibilities for future work include extending this technique to multi-channel systems so that clutter cancellation techniques may be used to mitigate the effect of clutter; applying spectral analysis techniques to estimate the number of human targets detected within a range bin; and using the Thalmann model to extract additional information about the target. For example, an estimate of the velocity/height ratio, RV, may be obtained and used, in conjunction with the velocity estimate, to extract an estimate of the person's height. Statistical properties of the variation of human height in men and women may then be used to classify targets according to gender.

References

[1] A.G. Yarovoy, L.P. Ligthart, J. Matuzas, and B. Levitas, "UWB radar for human being detection," *IEEE Aerospace and Electronic Systems Magazine*, Vol. 21, Issue 3, pp. 10-14, March 2006.

[2] D.G. Falconer, R.W. Ficklin, and K.G. Konolige, "Robot-mounted through-wall radar for detecting, locating, and identifying building occupants," *IEEE International Conference on Robotics and Automation*, Vol. 2, pp. 1868-1875, April 2000.

[3] A.M. Sabatini, and V. Colla, "A Method for Sonar Based Recognition of Walking People," *Robotics and Autonomous Systems*, Vol. 25, pp. 117-126, 1998.

[4] R.F. Weir, and D.S. Childress, "A new method of characterizing gait using a portable, real-time, ultrasound ranging device," *Proc. Of the 19th Annual International Conference of the IEEE Engineering in Medicine and Biology Society*, Vol. 4, pp. 1810-1812, Oct. 30-Nov.2, 1997.

[5] N.V. Boulgouris, D. Hatzinakos, and K.N. Plataniotis, "Gait Recognition: A challenging signal processing technology for biometric identification," *IEEE Signal Processing Magazine*, November 2005.

[6] J.L. Geisheimer, W.S. Marshall, E. Greneker, "A continuous-wave (CW) radar for gait analysis," *Signals, Systems and Computers*, Vol. 1, pp. 834-838, 2001.

[7] J.L. Geisheimer, E.F. Greneker, and W.S. Marshall, "A high-resolution Doppler model of human gait," *Proc. of SPIE, Radar Sensor Technology and Data Visualization*, Vol. 4744, 2002.
[8] P. van Dorp, and F.C.A. Groen, "Human walking estimation with radar," *IEE Proc. on Radar, Sonar, and Navigation*, Vol. 150, Issue 5, pp. 356-365, October 2003.
[9] R. Boulic, M.N. Thalmann, and D. Thalmann, "A global human walking model with real-time kinematic personification," *Visual Computing*, Vol. 6, pp. 344-358, 1990.
[10] M. Otero, "Application of a continuous wave radar for human gait recognition," *Proc. of SPIE, Signal Processing, Sensor Fusion and Target Recognition XIV*, Vol. 5809, pp. 538-548, 2005.
[11] Greneker, G., ``Very low cost stand-off suicide bomber detection system using human gait analysis to screen potential bomb carrying individuals", in *Proc. of SPIE*, Vol. 5788, 2005.
[12] S.Z. Gurbuz, W.L. Melvin, and D.B. Williams, "Detection and Identification of Human Targets in Radar Data," *Proc. of SPIE Defense and Security Symposium*, April 9-13, Orlando, FL, 2007.
[13] S.Z. Gurbuz, W.L. Melvin, and D.B. Williams, "Comparison of Radar-Based Human Detection Techniques," *41st Asilomar Conf. on Signals, Systems, and Computers*, Monterey, CA, November 4-7, 2007.
[14] F.C. Robey, D.R. Fuhrman, E.J. Kelly, and R. Nitzberg, "A CFAR Adaptive Matched Filter Detector," *IEEE Trans. on Aerospace and Electronic Systems*, Vol. 28, No. 1, Jan. 1992
[15] S.M. Kay, "Fundamentals of Statistical Processing, Vol. I: Detection Theory," Prentice Hall, 1993.
[16] S.M. Kay, "Fundamentals of Statistical Processing, Vol. I: Estimation Theory," Prentice Hall, 1993, pp. 531.

Sevgi Z. Gürbüz was born in Redwood City, CA, USA on November 8, 1976. She received the B.S. in Electrical Engineering and Computer Science with minor in Mechanical Engineering from the Massachusetts Institute of Technology (MIT) in June 1998. She received the M.Eng. in Electrical Engineering and Computer Science from MIT in February 2000. Currently, she is a PhD student at the Georgia Institute of Technology.

She received an Air Force Reserve Officer Training Corps (AFROTC) scholarship during her BS studies, a Charles Stark Draper Laboratory Fellowship during her MEng studies, and a National Defense Science and Engineering (NDSEG) Fellowship during her doctoral studies. From February 2000 to January 2004, she worked as a Radar Signal Processing Research Engineer at the Air Force Research Laboratory, Sensors Directorate, Rome, NY, USA.

She is a member of Eta Kappa Nu and Sigma Xi.

William Melvin (S'90-M'94-SM'99-F'08) is Director of the Sensors and Electromagnetic Applications Laboratory at the Georgia Tech Research Institute and an Adjunct Professor in Georgia Tech's Electrical and Computer Engineering Department. His research interests include digital signal processing with application to RF sensors, including adaptive signal processing for aerospace radar detection of airborne and ground moving targets, radar applications of detection and estimation theory, and synthetic aperture radar. He has authored over 135 publications in his areas of research interest and holds three patents on adaptive radar technology.

Dr. Melvin has served as a guest editor for several recent special sections appearing in the IEEE Transactions on Aerospace and Electronic Systems and acted as the Technical Co-Chair of the 2001 IEEE Radar Conference and 2004 IEEE Southeastern Symposium on System Theory. Dr. Melvin received a "Best Paper" award at the 1997 IEEE Radar Conference. He has provided tutorials and invited talks at a number of IEEE conferences and local IEEE section meetings on Ground Moving Target Indication, STAP fundamentals, and space-based radar. He is a regular reviewer for several IEEE and IET journal publications. Among his distinctions, Dr. Melvin is the recent recipient of the 2006 IEEE AESS Young Engineer of the Year Award, the 2003 US Air Force Research Laboratory Reservist of the Year Award, and the 2002 US Air Force Materiel Command Engineering and Technical Management Reservist of the Year Award. He was chosen as an IEEE Fellow for his contributions to adaptive radar technology.

Dr. Melvin received the Ph.D. in Electrical Engineering from Lehigh University in 1994, as well as the MSEE and BSEE degrees (with high honors) from this same institution in 1992 and 1989, respectively.

Douglas B.Williams (S'82–M'89–SM'03) received the BSEE, MS, and PhD degrees in electrical and computer engineering from Rice University, Houston, Texas. In 1989, he joined the faculty of the School of Electrical and Computer Engineering at the Georgia Institute of Technology, Atlanta, Georgia, where he is currently Professor and Associate Chair for Undergraduate Affairs. There he is also affiliated with the Center for Signal and Image Processing (csip.ece.gatech.edu) and the Arbutus Center for Distributed Engineering Education (www.cdee.gatech.edu).

Dr. Williams has served as an Associate Editor of the IEEE Transactions on Signal Processing and the EURASIP Journal of Applied Signal Processing. He is currently on the IEEE Signal Processing Society's Education Technical Committee, and he has been a member of the Society's Board of Governors and Signal Processing Theory and Methods Technical Committee. He has recently become a member of the ad hoc Lensing Oversight Committee for the IEEE Signal Processing Society/Connexions pilot project (www.ieeecnx.org). He is currently Area Editor—Special Issues for the IEEE Signal Processing Magazine and serves on the Magazine's Editorial Board. Dr. Williams was co-editor of the Digital Signal Processing Handbook published in 1998 by CRC Press and IEEE Press. He is a member of the Tau Beta Pi, Eta Kappa Nu, and Phi Beta Kappa honor societies.